

## CALCULATION OF HYDRODYNAMIC INTERACTION FORCES ON A SHIP ENTERING A LOCK USING CFD

S L Toxopeus and K Bhawsinka, Maritime Research Institute Netherlands (MARIN), The Netherlands

### SUMMARY

Estimation of hydrodynamic interaction forces experienced by a ship entering a lock plays an important role in the initial design phase of the lock. These forces govern the speed at which a ship can enter the lock and also the tug requirement for facilitating such manoeuvres. Hence hydrodynamic interaction forces can influence the turnaround time and the operational cost of the locks. Traditionally these forces have been calculated using model tests or by potential flow solvers. In this paper, a study is presented on predicting ship-lock interaction effects with the viscous-flow solver ReFRES-CO. The scenario consists of a large-beam bulk carrier entering the Pierre Vandamme Lock in Zeebrugge, Belgium. To validate the predictions, existing model tests are used. Furthermore, the results are compared to potential flow computations and CFD results from literature to highlight the benefits of each approach. The paper will show that with careful setup of the computations, reliable predictions of the ship-lock interaction effects can be obtained. In order to capture all physics of the interaction, viscous-flow computations are preferred above potential-flow predictions.

### NOMENCLATURE

|             |  |
|-------------|--|
| B           | Ship beam (m)  |
| $C_B$       | Block coefficient (-)                                    |
| $F_n$       | Froude number based on length (-)                        |
| $F_{n_h}$   | Froude number based on water depth (-)                   |
| h           | Water depth (m)  |
| $L_{oa}$    | Length overall (m)                                       |
| $L_{pp}$    | Length between perpendiculars (m)                        |
| T           | Ship draught (m)   |
| V           | Ship velocity (m/s)                                      |
| $V_t'$      | Total flow velocity $\sqrt{V_x^2 + V_y^2 + V_z^2}/V$ (-) |
| $V_{x,y,z}$ | Flow velocity in x, y, z direction (m/s)                 |
| $x_0$       | x-position of midship in lock geometry (m)               |
| X           | Longitudinal force (N)                                   |
| $y_0$       | y-position of midship in lock geometry (m)               |
| $y_{0CL}$   | y-position of centre line of lock geometry (m)           |
| Y           | Transverse force (N)                                     |
| N           | Yawing moment around midship (Nm)                        |
| $\beta$     | Drift angle (deg)  |
| $\Delta t$  | Computational time step size (s)                         |

### 1 INTRODUCTION

Estimation of hydrodynamic interaction forces experienced by a ship entering a lock plays an important role in the initial design phase of the lock. These forces govern the speed at which a ship can enter the lock and also the tug requirement for facilitating such manoeuvres. Hence hydrodynamic interaction forces can influence the turnaround time and the operational cost of the locks. Traditionally these forces have been calculated using model tests 12 or by potential flow solvers 3. However, with the development of computational tools, CFD is increasingly applied to predict the flow around ships during lock entry, see e.g. Wang and Zou 45, using deforming grids, or Meng and Wan 6, using overset grids.

In this paper, a study is presented on ship-lock interaction effects in which the viscous-flow solver ReFRES-CO

is used to predict the forces and moments on a ship while entering a lock. To model the motion of the ship entering the lock, a combined sliding and deforming grid approach is adopted. The scenario consists of a large-beam bulk carrier entering the Pierre Vandamme Lock in Zeebrugge, Belgium. To validate the predictions, model tests in a 1/75 scale lock configuration conducted by Flanders Hydraulics Research (FHR) are used 12. Furthermore, the results are compared to potential flow computations to highlight the benefits of each approach.

The paper will show that with careful setup of the computations, reliable predictions of the ship-lock interaction effects can be obtained. In order to capture all physics of the interaction, viscous-flow computations are preferred above potential-flow predictions.

### 2 EXPERIMENTAL DATA

A feasibility study for receiving a large beam bulk carrier in the Pierre Vandamme Lock (lock dimensions are 500m×57m×18.5m) in Zeebrugge was carried out in 1990s by Flanders Hydraulics Research (FHR) and Ghent University in Antwerp. During this study, systematic captive model tests were carried out in FHR's shallow water towing tank.

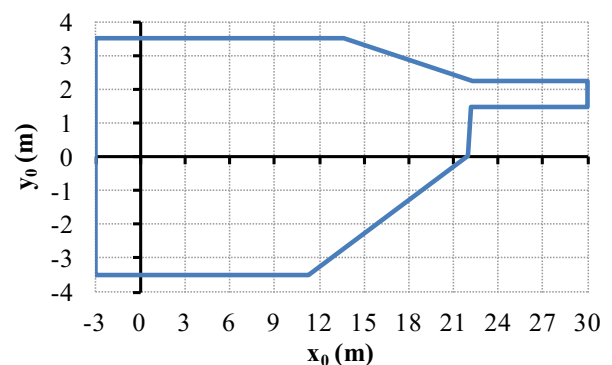


Figure 1. Overview of model lock geometry

**Table 1. Main particulars of bulk carrier**

| Designation                   | Symbol       | Prototype | Model |
|-------------------------------|--------------|-----------|-------|
| Length overall                | $L_{oa}$ (m) | 265.0     | 3.533 |
| Length between perpendiculars | $L_{pp}$ (m) | 259.2     | 3.456 |
| Beam                          | B (m)        | 43.0      | 0.573 |
| Draught                       | T (m)        | 17.342    | 0.231 |
| Block coefficient             | $C_B$ (-)    | 0.854     | 0.854 |

**Table 2. Overview of test cases**

| Case | Water depth to draught ratio $h/T$ (-) | Model speed $V$ (m/s) | Drift angle $\beta$ (deg) | Eccentricity $y_0 - y_{0CL}$ (m) |
|------|--|-----------------------|---------------------------|----------------------------------|
| G    | 1.2                                    | 0.15                  | 0                         | 0.00                             |
| H    | 1.2                                    | 0.10                  | -2                        | 0.00                             |

A 1/75 scale model of the lock configuration was constructed in the towing tank, with special attention to the asymmetric layout of the approach channel. FHR published a limited set of measurements as benchmark data, and more details of the measurements are given in Van Torre et al. 1.

For reference, a short description of the experimental data is repeated in this paper. An overview of the lock configuration as used in the towing tank for the captive model tests is given in Figure 1. The ship model was a 1/75 scale model of the bulk carrier *Mineral Antwerpen* with main dimensions listed in Table 1.

Results of three model tests were made available as benchmark data. During the tests, the model was equipped with a propeller and rudder, but the propeller was turned off. The variation of other parameters is shown in Table 2.

All tests started with the model's midship section at zero  $x_0$  position. After an acceleration phase, the model was towed with constant velocity from a midship position of  $x_0=2m$  until  $x_0=27.5m$  and was then decelerated over a distance of 0.5m. For each test, the forces and moments measured on the ship model and the vertical displacements of the fore and the aft perpendiculars were obtained 1. All results were provided in model scale dimensions and plotted as a function of the longitudinal position  $x_0$  of the model's midship section.

A ship-fixed coordinate system is used for determining ship kinematics and dynamics. The origin is located on the waterline, at half distance between the fore and the aft perpendiculars. The longitudinal x-axis is pointing ahead, the lateral y-axis is directed towards starboard, and the vertical z-axis is positive in downward direction. As a result, longitudinal forces are positive if directed ahead, lateral forces to starboard are positive, as are moments with the bow to starboard. Eccentricity with re-

spect to the lock centreline is positive if the ship is positioned to the starboard side of the centreline. Concerning vertical motions, a sinkage of the ship is considered to be positive. The drift angle is positive when the bow is turned to starboard.

### 3 COMPUTATIONAL TOOLS AND SETTINGS

#### 3.1 VISCOUS-FLOW SOLVER REFRESCO

##### 3.1 (a) Description

ReFRESCO is a viscous-flow CFD code that solves multiphase (unsteady) incompressible flows with the RANS equations, complemented with turbulence closure models, cavitation models and volume-fraction transport equations for different phases, see 7. The equations are discretised using a finite-volume approach with cell-centred collocated variables and in strong-conservation form. A pressure-correction equation based on the SIMPLE algorithm is used to ensure mass conservation as discussed by 8. Time integration is performed implicitly with first or second-order backward schemes. At each implicit time step, the non-linear system of velocity and pressure is linearised with Picard's method and either a segregated or coupled approach is used. In the latter, the coupled linear system is solved with a matrix-free Krylov subspace method using a SIMPLE-type preconditioner 8. A segregated approach is always adopted for the solution of all other transport equations. The implementation is face-based, permitting grids with elements consisting of an arbitrary number of faces (hexahedra, tetrahedra, prisms, pyramids, etc.), and, if needed, h-refinement i.e. hanging nodes. State-of-the-art CFD features such as moving, sliding and deforming grids, as well automatic grid refinement 9 are also available in the code.

For turbulence modelling, RANS/URANS, Scale Adaptive Simulation (SAS) 10, ((I)D)DES, Partially Averaged Navier Stokes (PANS) and LES approaches are available, see Pereira et al.11 12 13. The Spalart correction (proposed by Dacles-Mariani 14) to limit the production of turbulence kinetic energy based on the stream-wise vorticity can be activated. Automatic wall functions are available.

The code is parallelised using MPI and sub-domain decomposition, and runs on Linux workstations and HPC clusters. ReFRESCO is currently being developed, verified and validated at MARIN in the Netherlands in collaboration with IST (Lisbon, Portugal), USP-TPN (University of São Paulo, Brazil), Delft University of Technology, the University of Groningen, the University of Southampton, the University of Twente and Chalmers University of Technology.

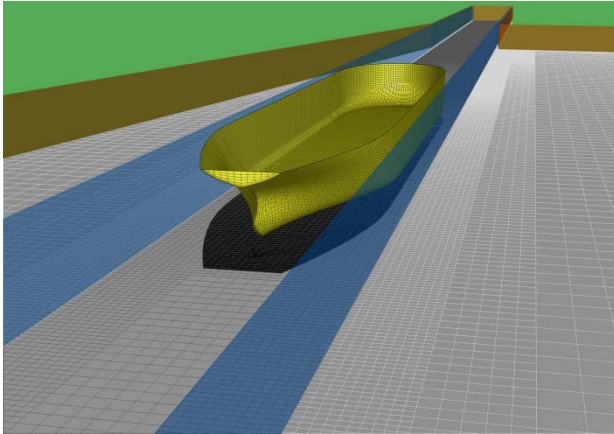


**Figure 2. Port side, ship and starboard domains. The interfaces between the domains are indicated in blue.**

### 3.1 (b) Computational domain and setup

To simplify the computations, free surface deformation, dynamic trim and sinkage, and the existence of the rudder and the propeller were neglected. Because of the very low speed during the experiments, i.e. the maximum Froude number was  $Fn=0.026$  and the maximum depth Froude number  $Fn_h=0.091$ , it can be expected that the influence of the free surface on the results is small. Furthermore, the non-rotating propeller is expected to mainly produce additional drag. The neglect of the rudder may cause some deviation between the computations and the measurements.

Unstructured grids with hexahedral cells were generated with HEXPRESS. Three domains were made: a domain on port side of the ship, a domain containing the ship and a domain on starboard side of the ship, see Figure 2. To facilitate the motion of the ship while entering the lock, the domain with the ship was deforming, with sliding interfaces between the deforming block and the (non-deforming) port and starboard domains. The deformation of the ship domain was realised using Radial Basis Functions 15.

The port and starboard domains were generated with more-or-less regular grids, but with additional refinement towards the interface in order to improve the transfer of information across the interface. The ship domain was generated with refinements towards the interfaces and towards the ship hull. The average  $y^+$  value was around 40 to 60, so wall functions were used to model the flow close to the hull surface. To maintain the grid quality during the full deformation of the grid for  $0 < x_0 < 27m$ , the grid was made with the ship at  $x_0=15.47m$  and subsequently the grid was deformed such that the computations could start with the ship at  $x_0=0m$ .

The size of the computational domain was the same as the lock geometry used during the experiments. On the hull surface, all external boundaries and the bottoms of the domains, no-slip boundaries were adopted.

At the undisturbed water surface, a symmetry boundary condition was applied.

**Table 3. Overview of grid densities**

|                        | Initial | Fine    |
|------------------------|---------|---------|
| Total cells            | 1645552 | 4646782 |
| Cells port domain      | 381114  | 1490780 |
| Cells ship domain      | 796368  | 1541248 |
| Cells starboard domain | 468070  | 1614754 |
| Faces on hull          | 12412   | 46590   |

Two grids were made: an initial grid with about 1.6 million cells, and a finer grid of about 4.6 million cells. Table 3 presents the number of cells in the grids and each domain and the number of faces used to represent the hull. The grid for case H was obtained using the grid of case G and rotating the ship by  $-2^\circ$  around the vertical axis through the midship, using mesh deformation.

For the present computations, use was made of the  $k-\omega$  SST turbulence model 16 and a second order accurate time discretisation.

## 3.2 POTENTIAL-FLOW SOLVER ROPES

### 3.2 (a) Description

ROPES has been developed for the prediction of ship-ship interaction forces in shallow water of arbitrary depth. The computational method used in ROPES is based on three-dimensional potential flow and the double-body assumption. This means that free-surface effects of vessels are not accounted for. Furthermore, trailing wakes are not used in ROPES, so the potential flow model does not include lift effects. The flow equations are solved using standard zero-order panels and Rankine sources with or without the effect of restricted water depth and channel walls (see Pinkster 17 and Korsmeyer et al. 18). Based on the solution of the source strengths on the panels describing the various bodies, the hydrodynamic forces on the ships are computed with equations developed by Xiang and Faltinsen 19. These equations are used to compute the complete set of hydrodynamic forces on all bodies. ROPES is applicable to multi-body simulation scenarios involving various ships and port structures.

### 3.2 (b) Computational domain and setup

A close up view of the panel distribution on the hull and on the lock surface is given in Figure 3. The hull is represented using 1650 panels, while 2091 panels are used to describe the lock surface. For simplicity, the rudder and propeller have not been considered in the ROPES computations. The computations were made for full scale conditions and the interaction force and moment results were obtained. These results were then scaled to obtain model scale results.

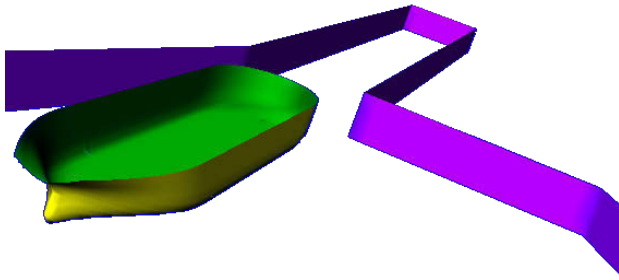


Figure 3. Panelling for ROPES potential flow computation, case G

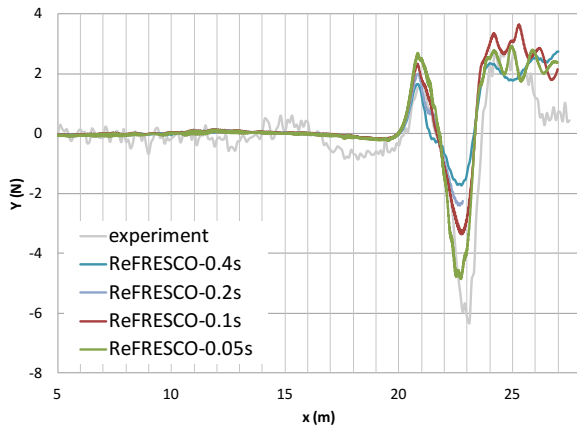


Figure 4. Influence of time step on transverse force, case G, initial grid

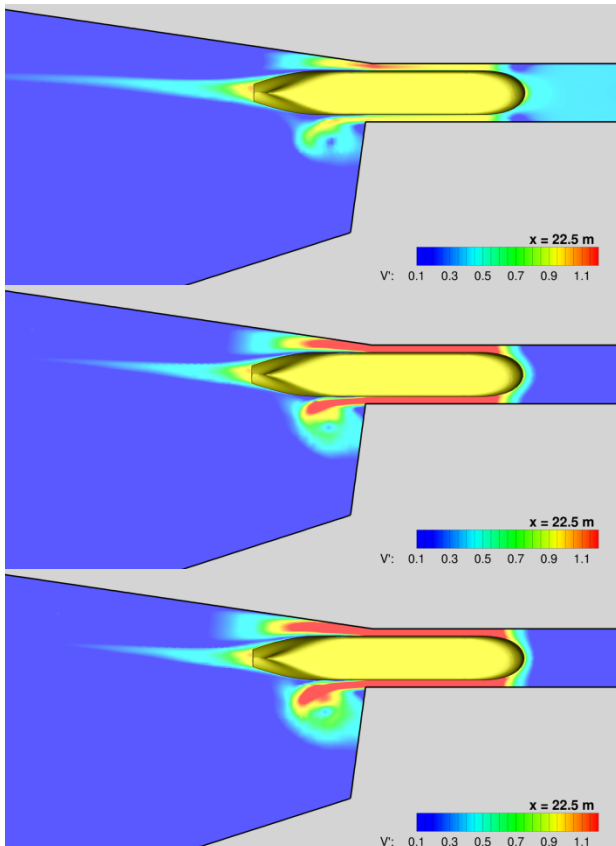


Figure 5. Visualisation of the total velocity field  $V_t'$  at the water surface for  $\Delta t=0.4s$  (top),  $\Delta t=0.1s$  (middle) and  $\Delta t=0.05s$  (bottom), case G, initial grid,  $x_0=22.5m$

## 4 RESULTS

### 4.1 REFRESKO SOLUTION VERIFICATION

#### 4.1 (a) Iterative convergence

During each time step, the RMS of the residuals were reduced about 4 orders of magnitude. It was found that during the approach phase, lower residuals could be obtained than with the ship near or in the lock entry. This is caused by the increased complexity of the flow when entering the lock.

#### 4.1 (b) Discretisation in time

It was found that the ReFRESKO results were very dependent on the chosen computational time step  $\Delta t$  during the stage of entering the lock entrance, see Figure 4 for the case G results. Therefore ReFRESKO runs were made for various time steps (ranging from 0.4s to 0.025s) to check the influence of the discretization in time. Satisfactory results were obtained for 0.05s time steps. Calculations with an even smaller time step of 0.025s did not improve the results. Figure 5 shows the  $V_t'$  velocity field around the ship at a specific position during the case G computation. It is seen that by reducing the time step, significantly different and more complex physics are captured.

Also for case H, the time step size was varied for the computations with the initial grid. The influence of the time step size on the transverse force can be seen in Figure 6. For the flow field, the results are shown for two different time steps in Figure 7. Again, satisfactory results were obtained for  $\Delta t=0.05s$ .

For the lock approach (up to around  $x_0=17m$ ), a time step size of 0.2s appeared to be sufficient. Therefore, all subsequent simulations were done with a time step  $\Delta t$  of 0.2s ( $\approx 1/115 L_{pp}/V$ ) for  $0 < x_0 < 17m$  and 0.05s ( $\approx 1/460 L_{pp}/V$ ) for  $x_0 > 17m$ .

#### 4.1 (c) Discretisation in space

For case G and H, two different grid sets were used. Some influence of the grid density was seen in the longitudinal force  $X$  and marginally in the transverse force and yawing moment for case G, see Figure 8. For these grid densities, the discretisation error due to space was found to be smaller than the error due to discretisation in time.

Also for case H, the influence of the grid was studied, see Figure 9 and a similar grid dependency was observed.

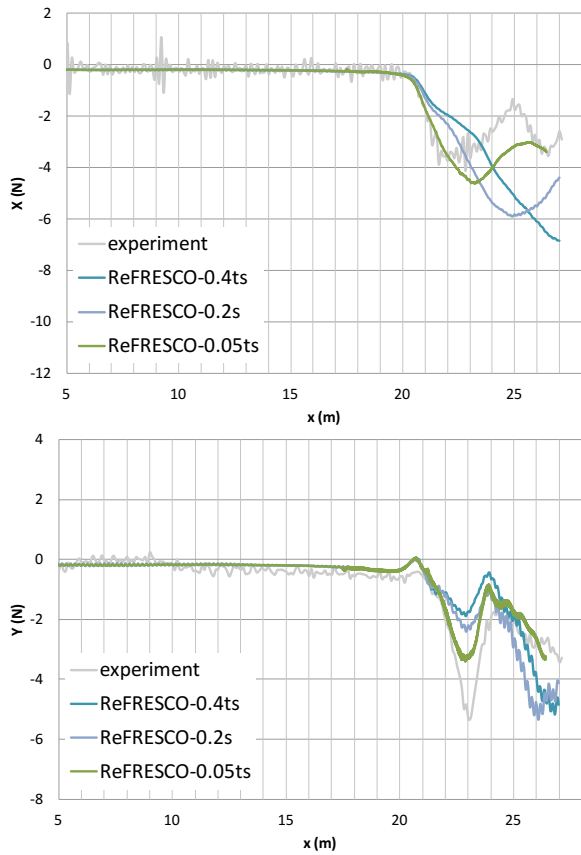


Figure 6. Influence of time step on transverse force, case H, initial grid

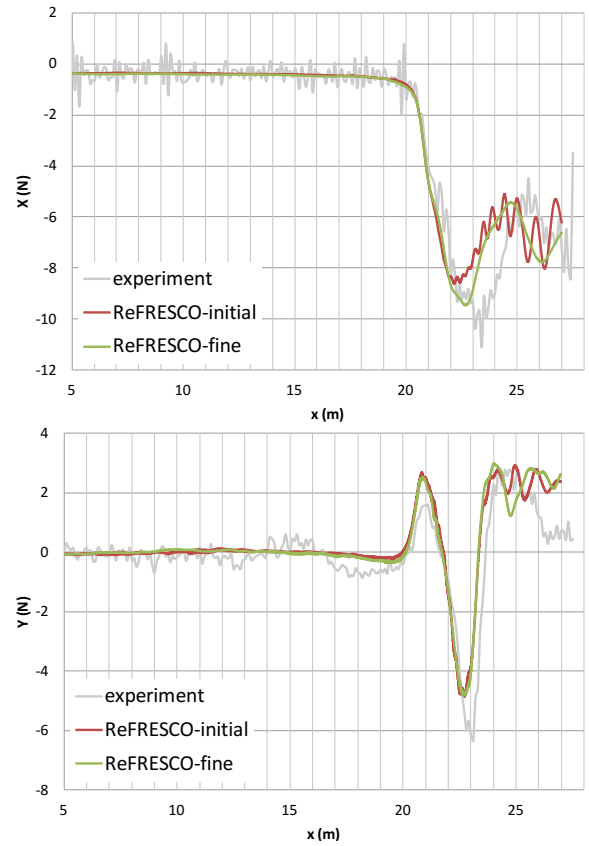


Figure 8. Influence of grid density on longitudinal (top) and transverse force (bottom), case G,  $\Delta t=0.05s$

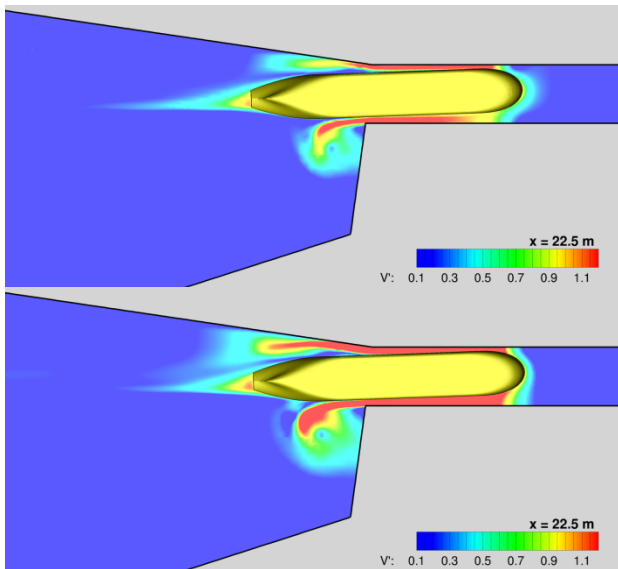


Figure 7. Visualisation of the total velocity field  $V_t'$  at the water surface for  $\Delta t=0.2s$  (top) and  $\Delta t=0.05s$  (bottom), case H, initial grid,  $x_0=22.5m$

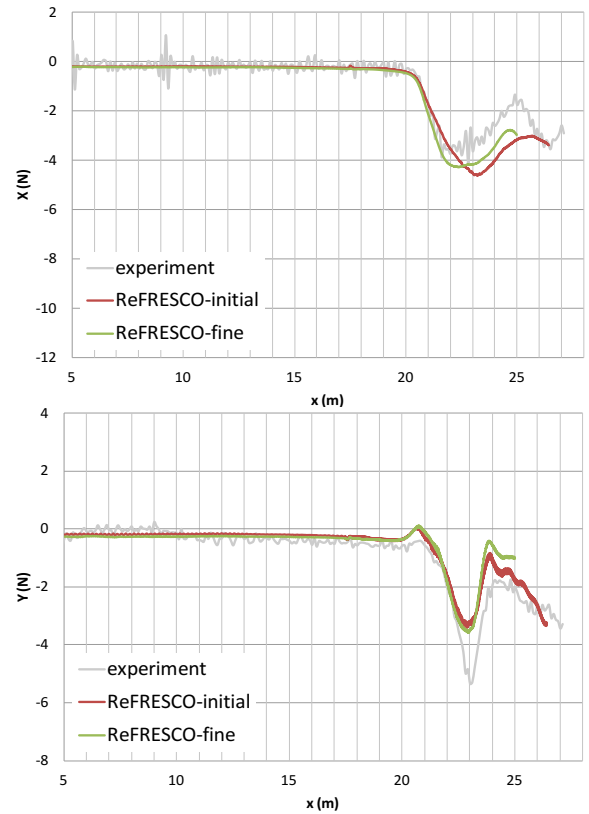


Figure 9. Influence of grid density on longitudinal (top) and transverse force (bottom), case H,  $\Delta t=0.05s$

## 4.2 DISCUSSION OF THE FLOW

To better understand the flow during the lock entry, the absolute flow velocity  $V_t$  around the ship calculated by ReFRESKO with a calculation time step of  $\Delta t=0.05s$  is plotted in Figure 10 and Figure 12 for case G and in Figure 11 and Figure 13 for case H, for positions of the midship of  $x_0=19.5, 20.5, 21.5, 22.5$  and  $23.5m$ . These plots give an indication of the development of the flow as the ship enters the lock.

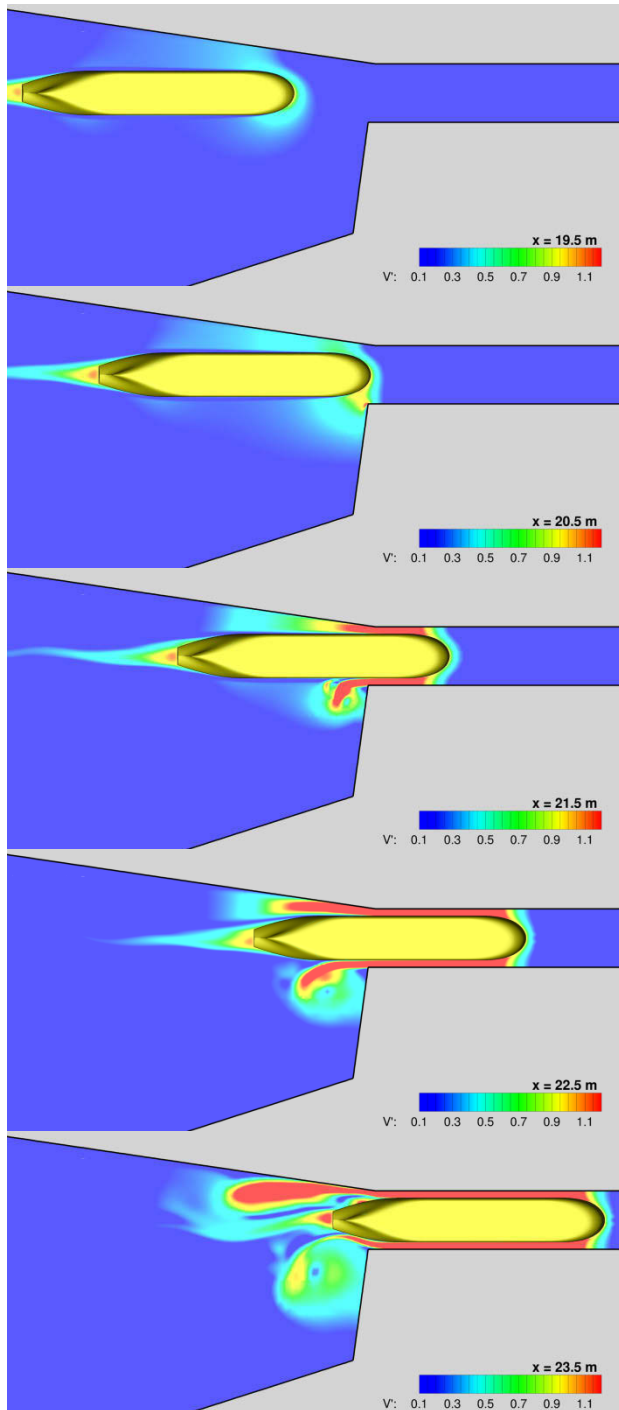


Figure 10. Visualisation of the total velocity field at the water surface, case G, fine grid,  $\Delta t=0.05s$

First looking at case G, the asymmetry in the flow due to the asymmetric approach channel design can be seen: at port side, higher velocities can be observed than at starboard. Initially, this results in a slight suction force towards port side (see the evolution of the forces in Figure 14). At  $x_0=20.5m$ , the bow reaches the lock gate and a large flow velocity develops between the bow and the starboard side of the lock entrance. A strong side force is generated, combined with a positive yawing moment, both pulling the bow to starboard.

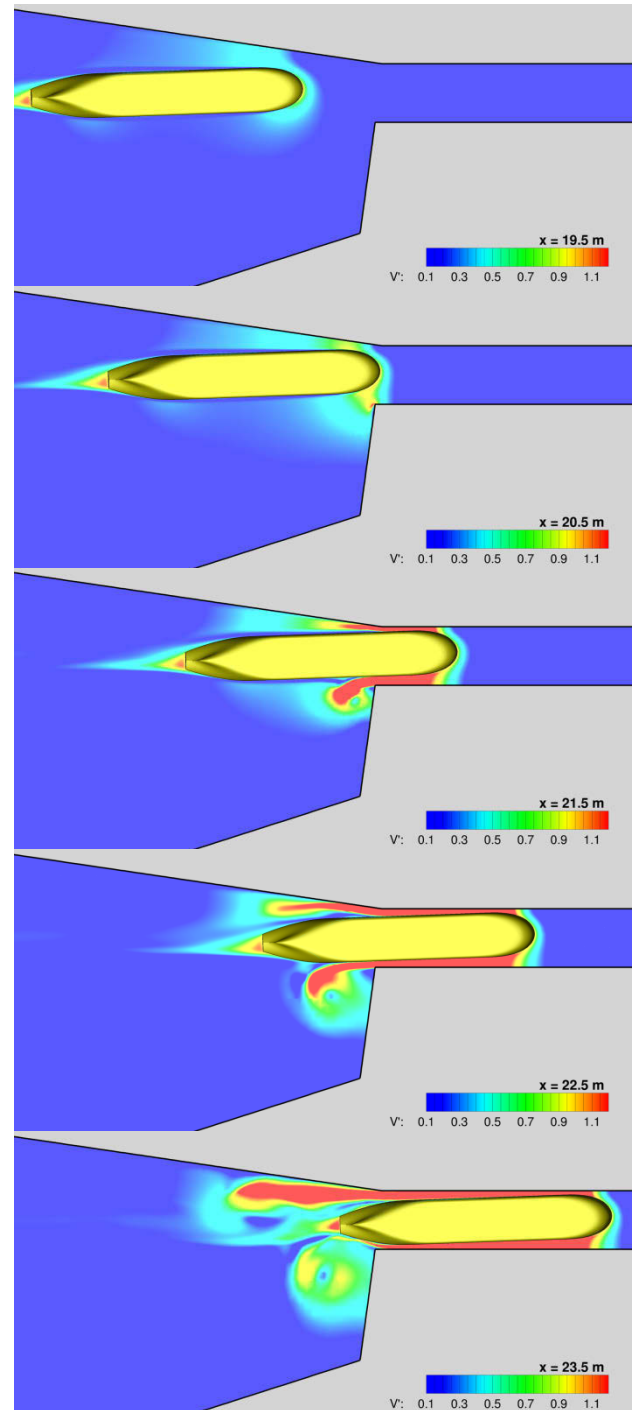


Figure 11. Visualisation of the total velocity field at the water surface, case H, fine grid,  $\Delta t=0.05s$

When the ship moves further, the water in the lock is pushed outward due to the displacement of the ship and it accelerates around the hull. At port side, the flow along the harbour walls follows the wall without separating, but at starboard, the sharp edge between the lock wall and harbour wall induces a separation of the out flow of the lock and subsequently a large eddy is generated.

These eddies have more space to mix and dissipate with the surrounding flow than the accelerated flow on port side. A large region of return flow develops on port side and with the ship at  $x_0=22.5\text{m}$ , the accelerated flow extends along the complete length of the ship. Therefore a suction force towards port side is acting on the hull, in combination with a yawing moment pulling the stern to port side.

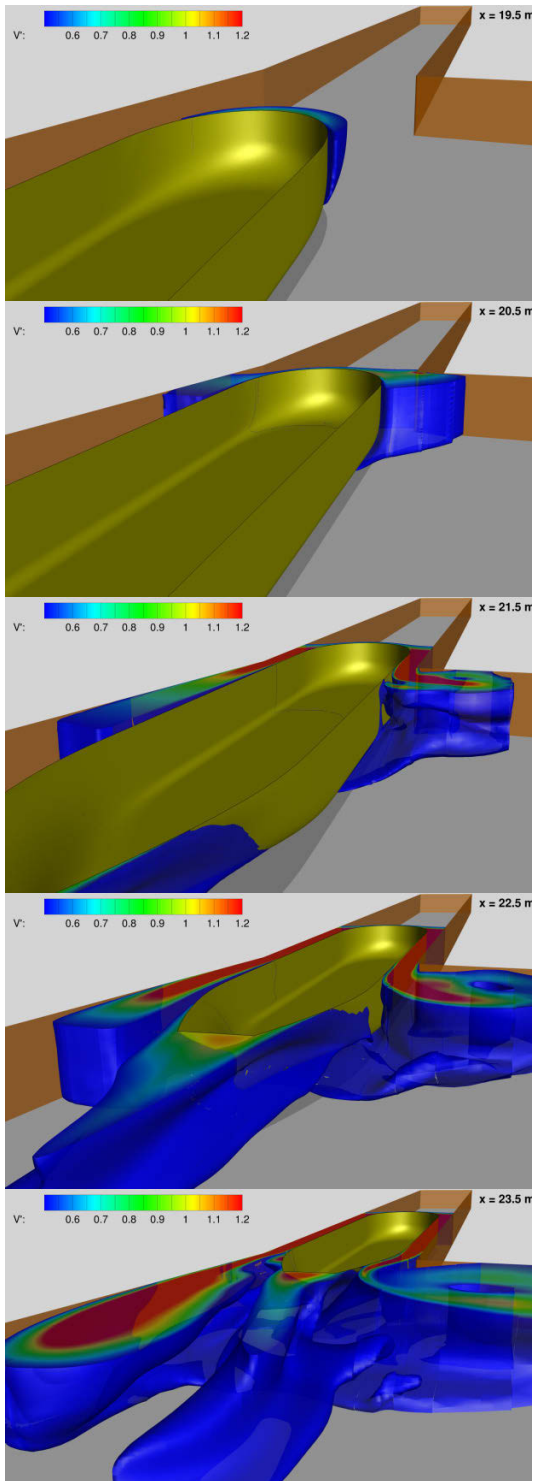


Figure 12. Isosurface of  $V_i' \geq 0.5$ , coloured by  $V_i'$ , for several longitudinal positions of the model, case G, fine grid,  $\Delta t=0.05\text{s}$

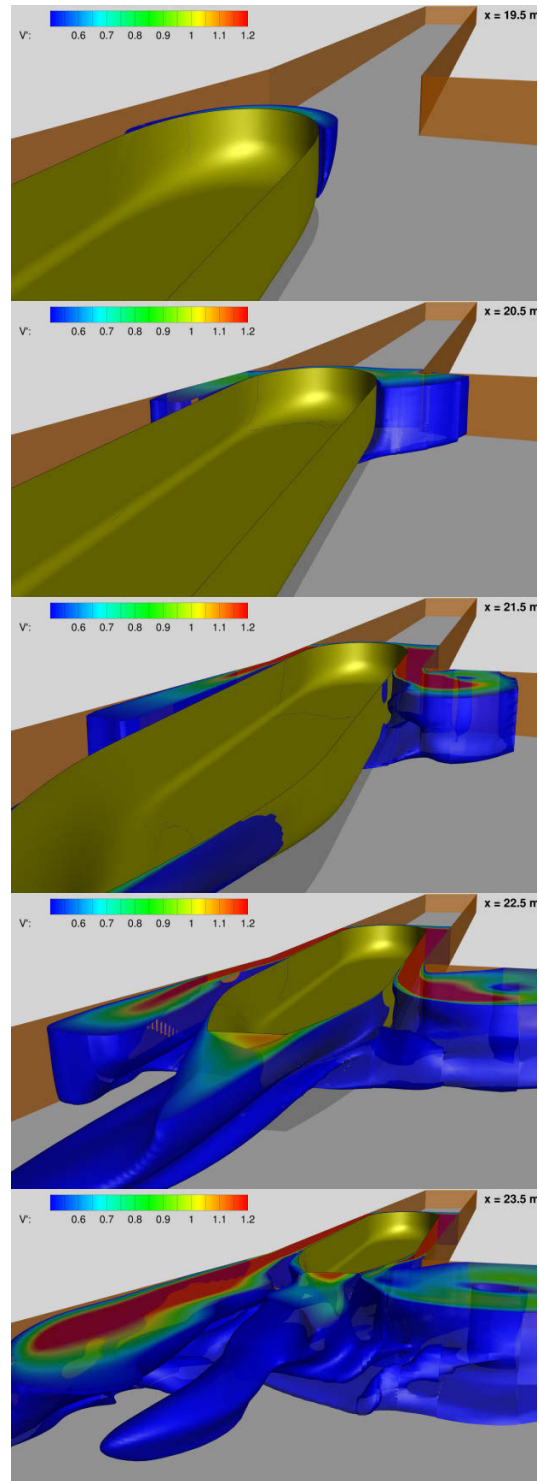


Figure 13. Isosurface of  $V_i' \geq 0.5$ , coloured by  $V_i'$ , for several longitudinal positions of the model, case H, fine grid,  $\Delta t=0.05\text{s}$

When the stern enters the lock, around  $x_0=23.5\text{m}$ , the accelerated flow on starboard side follows the shape of the stern without separation, while the flow on port side, with a slightly higher velocity, cannot remain attached and separates from the stern. This generates a low pressure region at the starboard side of the stern and a higher pressure on port side, pushing the stern towards starboard.

For case H, in which the ship sails with a drift angle  $\beta$  of  $-2$  deg, similar flow physics are observed. However, due to the drift angle, the distance between the hull and the lock walls becomes smaller and larger flow gradients occur.

### 4.3 COMPARISON WITH THE EXPERIMENTS

A comparison of the forces and moment computed by ReFRESKO (fine grid,  $\Delta t=0.05\text{s}$ ) and ROPES with the experiments for case G is given in Figure 14. It is seen that the ReFRESKO results match very well with the model test results both in terms of trends. The agreement in terms of absolute values is reasonable, although the peak values are not exactly captured. The observed differences can probably be attributed partly to numerical or experimental errors, but also to the neglect of the dynamic trim and sinkage, the free surface deformation, and the propeller and rudder not being incorporated in the CFD results.

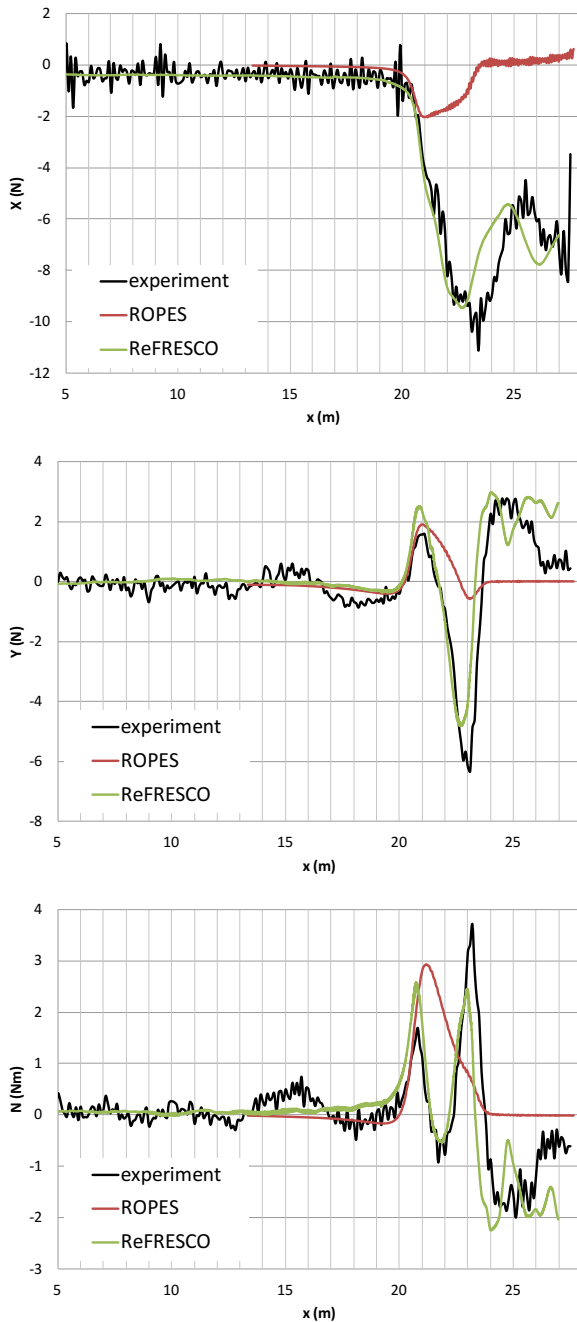


Figure 14. Forces and moment, case G

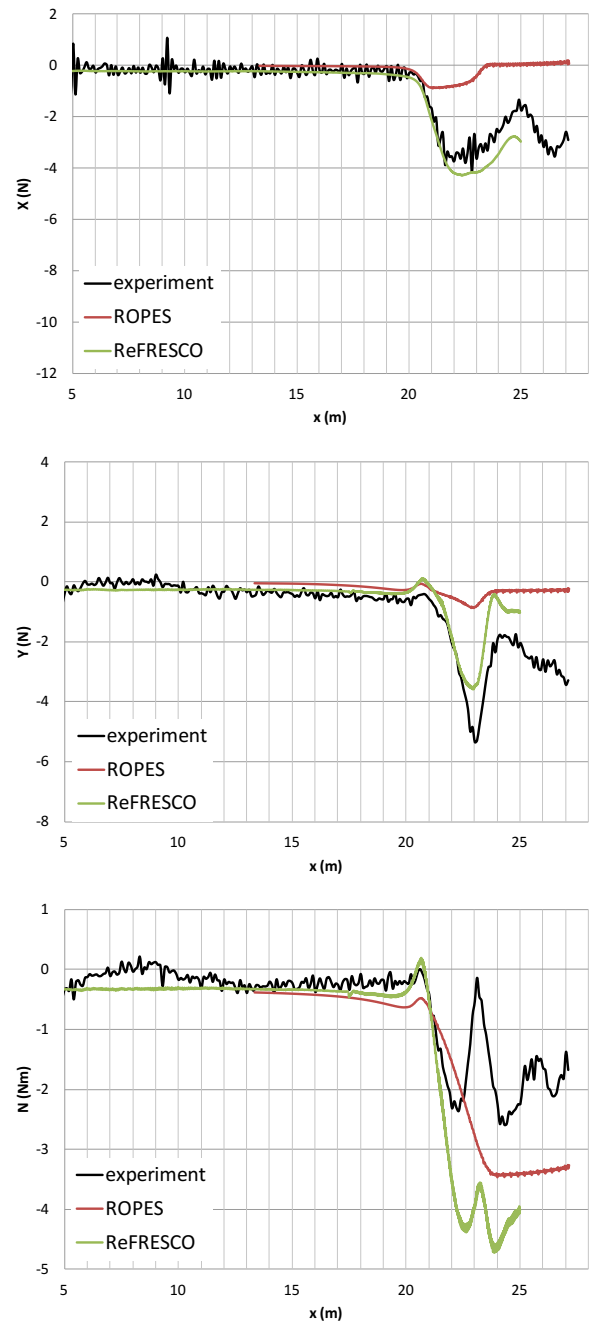


Figure 15. Forces and moment, case H

This demonstrates that even when neglecting the free surface deformation reasonable predictions of the physics of the lock entry can be obtained. The common explanation of a travelling free surface wave in the lock being the primary reason for the large interaction effects can apparently not be applied to the present case.

The comparison for case H is shown in Figure 15. The agreement between the ReFRESKO predictions (fine grid,  $\Delta t=0.05s$ ) and the experiments is reasonable for the longitudinal and transverse forces, although also in this case the peak values are not fully captured. However, the agreement of the yaw moment from CFD with the experiments is rather poor, especially when a large portion of the ship is located inside of the lock. This may be caused by the use of a grid that is still coarse near the interface. In particular near the port side of the bow, the grid on both sides of the interface between the port side domain and the ship domain is insufficiently fine to allow accurate interpolation of the flow information across the interface between the two domains. Further computations with a more refined grid, with  $\Delta t=0.05s$ , are recommended.

From these plots, it is found that ROPES highly under predicts the X force. For the hydrodynamic sway force and yaw moment, ROPES only captures the initial interaction effects when the bow reaches the lock entrance, but completely fails to predict the full physics of the flow when the ship is partly or fully into the lock. This demonstrates that viscosity dominates the interaction effects inside the lock, which cannot be captured with a purely potential flow computation.

## 5 CONCLUSIONS

In the present paper, unsteady CFD computations for a ship entering a lock are presented. Use is made of sliding and deforming grids to model the motion of the ship in the lock geometry. Two cases were considered: one case with the ship entering the lock without drift angle, and a case in which the ship moved at a drift angle of -2 deg. It is found that the results strongly depend on the time step. For the case with drift angle, the results showed also a grid dependency and further studies are required to see whether a finer grid, in combination with the appropriate time step will result in better agreement between the predictions and the experiments.

It was found that the CFD computations are able to capture the physics of the flow during the lock entry manoeuvre. Even without modelling the free surface, the predicted forces and moments acting on the ship entering the lock without drift angle were close to the experimental data. This shows that the common explanation of a travelling free surface wave in the lock being the primary reason for the large interaction effects can apparently not be applied to the present case. Computations with a potential flow code demonstrated that the interaction effects inside the lock are of a very

viscous nature, which cannot be captured with a purely potential flow computation.

From the outcome of the study, it can be concluded that with unsteady viscous-flow computations, the trends in the hydrodynamic interactions experienced by a ship entering a lock can be predicted well. To be able to quantitatively predict the peak loads during lock entries, further studies are required.

## 6 ACKNOWLEDGEMENTS

This work has been performed in the context of the *TO2 (Toegepast Onderzoek Organisaties) Natte Kunstwerken van de Toekomst* project.

## 7 REFERENCES

1. Vantorre, M.; Delefortrie, G.; Mostaert, F. (2012). Behaviour of ships approaching and leaving locks: Open model test data for validation purposes. *Version 2\_1, WL Rapporten, WL2012R815\_08e*, Flanders Hydraulics Research and Ghent University - Division of Maritime Technology, Antwerp, Belgium.
2. Vantorre, M.; Delefortrie, G. (2013). Behaviour Of Ships Approaching And Leaving Locks: Open Model Test Data For Validation Purposes, *3<sup>rd</sup> International Conference on Ship Manoeuvring in Shallow and Confined Water: with non-exclusive focus on Ship Behaviour in Locks*, Ghent, Belgium, pp. 337-352.
3. Pinkster, J.A.; Bhawsinka, K. (2013). A real-time simulation technique for ship-ship and ship-port interactions, *28<sup>th</sup> International Workshop on Water Waves and Floating Bodies*, L'Isle sur la Sorgue, France.
4. Wang, H.-Z.; Zou, Z.-J. (2013) Numerical study on hydrodynamic behaviour of ships sailing in locks, *3<sup>rd</sup> International Conference on Ship Manoeuvring in Shallow and Confined Water: with non-exclusive focus on Ship Behaviour in Locks*, Ghent, Belgium, pp. 129-134.
5. Wang, H. Z.; Zou, Z. J. (2014). Numerical study on hydrodynamic interaction between a berthed ship and a ship passing through a lock, *Ocean Engineering*, 88: pp. 409-425. doi:10.1016/j.oceaneng.2014.07.001.
6. Meng, Q.; Wan, D. (2015). Numerical Simulations of Viscous Flows around a Ship While Entering a Lock With Overset Grid Technique, *Twenty-fifth International Ocean and Polar Engineering Conference (ISOPE)*. Kona, Big Island, Hawaii.
7. Vaz, G.; Jaouen, F. A. P.; Hoekstra, M. (2009). Free-Surface Viscous Flow Computations. Validation of URANS Code FreSCo, *28<sup>th</sup> International Conference on Ocean, Offshore and Arctic Engineering*

- (*OMAE*), Honolulu, Hawaii,  
doi:10.1115/OMAE2009-79398.
8. Klaij, C. M.; Vuik, C. (2013). SIMPLE-type preconditioners for cell-centered, colocated finite volume discretization of incompressible Reynolds-averaged Navier-Stokes equations, *International Journal for Numerical Methods in Fluids*, 71(7): pp. 830-849, doi:10.1002/flid.3686.
  9. Windt, J.; Bosschers, J. (2015). Influence Of Local And Adaptive Mesh Refinement On The Tip Vortex Characteristics Of A Wing And Propeller, *VI International Conference on Computational Methods in Marine Engineering (MARINE 2015)*, Rome, Italy.
  10. Menter, F. R.; Egorov, Y. (2005). A Scale-Adaptive Simulation Model using Two-Equation Models, *43<sup>rd</sup> AIAA Aerospace Sciences Meeting and Exhibit*, Reno, Nevada.
  11. Pereira, F. S.; Vaz, G.; Eça, L. (2014). On the use of Hybrid Turbulence Models, *17<sup>th</sup> Numerical Towing Tank Symposium (NuTTS)*, Marstrand, Sweden, pp. 135-140.
  12. Pereira, F. S.; Vaz, G.; Eça, L. (2015). On The Numerical Requirements Of RANS And Hybrid Turbulence Models, *VI International Conference on Computational Methods in Marine Engineering (MARINE 2015)*, Rome, Italy.
  13. Pereira, F. S.; Vaz, G.; Eça, L. (2015). An assessment of Scale-Resolving Simulation models for the flow around a circular cylinder, *8<sup>th</sup> International Symposium on Turbulence, Heat and Mass Transfer (THMT'15)*, Sarajevo, Bosnia and Herzegovina.
  14. Dacles-Mariani, J.; Zilliac, G. G.; Chow, J. S.; Bradshaw, P. (1995). Numerical/experimental study of a wingtip vortex in the near field, *AIAA Journal*, 33(9): pp. 1561-1568, doi:10.2514/3.12826.
  15. Rendall, T.; Allen, C. (2009). Efficient mesh motion using radial basis functions with data reduction algorithms, *Journal of Computational Physics*, 228(17): pp. 6231-6249, doi:10.1016/j.jcp.2009.05.013.
  16. Menter, F. R.; Kuntz, M.; Langtry, R. (2003). Ten Years of Industrial Experience with the SST Turbulence Model, *Fourth International Symposium on Turbulence, Heat and Mass Transfer*, Antalya, Turkey.
  17. Pinkster, J.A. (2004). The Influence of a Free Surface on Passing Ship Effects, *International Ship Building Progress*, 51(4): pp. 313-338.
  18. Korsmeyer, F.T., Lee, C.-H.; Newman, J.N. (1993). Computation of Ship Interaction Forces in Restricted Waters, *Journal of Ship Research*, 37(4): pp 298-306.
  19. Xiang, X.; Faltinsen, O.M. (2010). Maneuvering of Two Interacting Ships in Calm Water, *11<sup>th</sup> International Symposium on Practical Design of Ships and Other Floating Structures (PRADS)*, Rio de Janeiro, Brazil.

## 8 AUTHORS' BIOGRAPHIES

**Serge Toxopeus** is a Senior Researcher, Research Coordinator of the Manoeuvring and Nautical studies and Team leader of the R&D CFD Development team at MARIN. He is mainly involved in the development of CFD for manoeuvring applications, including the influence of confined water due to banks or shallow water.

**Karan Bhawsinka** is a Project Manager at MARIN's nautical centre MSCN. He is mainly involved in research and consultancy projects which use MARIN's full mission bridge and desktop simulators. He specialises in manoeuvring simulations with special focus on shallow and confined water manoeuvres.